Novel Photoactive Spirooxazine Based Switch@MOF Composite Materials

Heidi A Schwartz, Melanie Werker, Christian Tobeck, Ronja Christoffels, Dominik Schaniel, Selina Olthof, Klaus Meerholz, Holger Kopacka, Hubert Huppertz, Uwe Ruschewitz

ChemPubSoc Europe

DOI: 10.1002/cptc.201900193

CHEMPHOTOCHEM Articles

Novel Photoactive Spirooxazine Based Switch@MOF Composite Materials

Heidi A. Schwartz,[a, d] Melanie Werker,[a] Christian Tobeck,[a] Ronja Christoffels,[a] Dominik Schaniel,[b] Selina Olthof,[c] Klaus Meerholz,[c] Holger Kopacka,[d] Hubert Huppertz,[d] and Uwe Ruschewitz*[a]

Molecules, which reversibly transform between two structural configurations upon excitation with electromagnetic radiation, are attractive candidates for the design of smart materials e.g. memory devices. A possible approach for the development of such smart materials is the construction of hybrid systems that contain these photochromic molecules as well as a porous host matrix, which enables their switching process in the solid state. We herein present the first light-responsive materials consisting of the photoswitchable spirooxazine 1,3,3-trimethyl indolinonaphthospirooxazine (SP–O) and crystalline porous MOF (metal–organic framework) hosts, namely MOF-5, MIL-68(In), MIL-68 (Ga), and MIL-53(Al), which were combined to form hybrid SP–O@MOF composites. These systems show a reversible photochromic response and host-dependent absorption maxima of the incorporated guest molecules. Most remarkably, SP–O is extremely photostable upon repetitive and prolonged UV light exposure especially inside MOF-5, making these composite materials attractive candidates for potential applications in data storage devices.

1. Introduction

The synthesis and design of functional hybrid switch@MOF materials has become a central point of research in recent years.[1,2] These smart composites are obtained by introducing photoswitchable dye molecules such as azobenzenes and (fluorinated) derivatives,[3–8] diarylethenes[9] or spiropyrans[10–12] as non-covalently attached guests into the crystalline porous MOF (metal-organic framework) host scaffold.

Photoswitchable molecules undergo the phenomenon called photochromism, which is defined as the reversible light induced structural transformation of a species between two configurations, which differ in their absorption properties.[13] Depending on the nature of the photochromic dye, light induced changes cause *E*/*Z* isomerizations (azobenzenes) or ring-opening/-closing reactions (spiropyrans or diarylethenes). Reconversion to the ground state is either reached by irradiation with light of another wavelength or heat supply.[14] The light induced structural changes require a certain degree of sterical freedom, which is only barely given in the dense packing of these molecules in their crystalline state. Therefore, the embedment into porous hosts like MOFs is an elegant way to enable the isomerization processes without the necessity of a solvent or an amorphous polymer matrix.

MOFs are hybrid materials, consisting of inorganic nodes, mostly metal cations or metal-oxo-clusters, which are linked by organic linker molecules/anions with at least two functional groups, forming a three dimensional framework with potential voids.[15] Especially because of these voids, MOFs are extremely promising candidates for both industry and science. If accessible, these voids offer various applications e.g. gas adsorption,[16,17] separation of gases[18,19] and liquids,[19–21] heterogeneous catalysis,[22] drug encapsulation and delivery,[23,24] and for electronic devices.[25,26] These diverse applicabilities are the result of the structural design of MOFs. The organic linker molecules/anions as well as the metal nodes can be variably tailored. *Yaghi* and co-workers synthesized isoreticular MOFs (IR-MOFs), which show the same network topology by simultaneous elongation or substitutional variation of the linkers.[27] The systematic design and functionalization of MOF pores is an interesting feature of this class of materials. As a result of these modifications, the accessible voids possess different physicochemical environments, which make them promising candidates to control guest uptake and host-guest interactions. While most applications focus on gas adsorption and storage,

[a] *Dr. H. A. Schwartz, M. Werker, C. Tobeck, R. Christoffels, Prof. Dr. U. Ruschewitz*
Institute of Inorganic Chemistry
University of Cologne
Greinstraße 6, 50939 Cologne (Germany)
E-mail: uwe.ruschewitz@uni-koeln.de
[b] *Prof. Dr. D. Schaniel*
Université de Lorraine, CNRS, CRM²
Boulevard des Aiguillettes, BP 70239
54506 Vandoeuvre les Nancy (France)
[c] *Dr. S. Olthof, Prof. Dr. K. Meerholz*
Institute of Physical Chemistry
University of Cologne
Greinstraße 4–6, 50939 Cologne (Germany)
[d] *Dr. H. A. Schwartz, Dr. H. Kopacka, Prof. Dr. H. Huppertz*
Institute of General, Inorganic, and Theoretical Chemistry
University of Innsbruck
Center for Chemistry and Biomedicine
Innrain 80–82, 6020 Innsbruck (Austria)

Supporting information for this article is available on the WWW under https://doi.org/10.1002/cptc.201900193

combining MOFs and photoswitches has only been given increasing attention in the recent past.[1,2] Different photochromic dyes were embedded into MOFs: stilbenes,[28] 2-(phenylazo)pyridine,[29,30] azobenzenes and (fluorinated) derivatives,[3–8] diarylethenes,[9] or spiropyrans.[10–12] Surprisingly, so far spirooxazines as non-covalently attached switchable guest molecules or as part of the framework itself have not been considered at all, even though they feature promising photophysical properties.

Spiropyrans and spirooxazines are closely related to each other. Both dye molecules differ in their structure only by an additional nitrogen atom in the spiropyran chromene ring. Hence, the spiro carbon connects the indoline with a benz

oxazine part in spirooxazines. While spiropyrans were very intensively studied after their discovery,[31,32] the synthesis of and publications on spirooxazines somehow went unnoticed, even though they are known since 1960.[33] Only since the 1980s, the class of spirooxazines has become more present, mainly due to *Chu*'s discovery of the extraordinary photostability of 1,3,3-trimethylindolino-naphthospirooxazine (SP–O) and derivatives under continuous light excitation.[33] For this reason, spirooxazines should be preferred to spiropyrans in many possible applications. Upon UV light irradiation, the closed spirooxazine form converts into the open strongly coloured merocyanine form. The switching process of SP–O is depicted in Figure 1.

Excited spirooxazine exhibits an absorption maximum in the range $\lambda = 480–670$ nm, which is dependent on the substituents and the polarity of the surrounding medium (solvatochromism). Besides, the absorption maxima feature an asymmetric shape with a red- or blue-shifted shoulder for different substituents under ambient conditions.[33] Solvatochromism can either be positive or negative in dependence of the substituents of the spirooxazine molecules. For SP–O, positive solvatochromism was found, which results in batho chromically shifted absorption bands.[33] The combined photochromic and solvatochromic response of spirooxazines makes them promising candidates for the design of functional hybrid materials.

Therefore, it was the aim of the present work to synthesize and characterize different SP–O@MOF systems to examine the influence of the MOF hosts on the optical and photoswitching properties of the embedded spirooxazine molecules. Notably, the SP–O molecules will be non-covalently bound to the MOF framework rather than being attached to the MOF scaffold,[34–36] as a part of the linker backbone[35,37–40] or as a substituent of the linker,[41–50] which necessarily leads to a high mobility of the dye molecules in the former. That way, host-guest and guest-guest

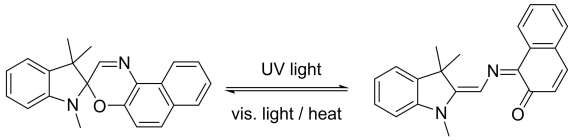

Figure 1. Light-induced photoisomerization of SP–O from its closed SP form to its open MC form (SP–O to MC–O photoconversion).

interactions are expected to have an important impact on the photophysical properties of these composites, but on the other hand can be examined in an elegant way in these systems.

2. Results and Discussion

The spirooxazine SP–O was incorporated into MOF-5 ($Zn_4O(bdc)_3$),[51] MIL-68(In) (In(OH)(bdc)),[52] MIL-68(Ga) (Ga(OH)(bdc)),[52] and MIL-53(Al) (Al(OH)(bdc))[53] via a gas phase loading process to exclude any influence from solvent molecules throughout this work. All host materials contain the same linker molecule bdc^{2-} ($H_2bdc = C_8H_6O_4$, 1,4-benzenedicarboxylic acid = terephthalic acid) to focus our investigations on the influence of the metal-node as well as the shape and the size of the MOF pores. Furthermore, the selected host materials meet the following requirements:

1) The pore opening and the pore size of the MOF scaffold is large enough to enable incorporation and isomerization processes of the spirooxazine dyes (for detailed information on the respective sizes see Supporting Information).
2) The absorption bands of the MOF hosts should not overlap with the ones of the SP–O molecule so that the switching processes can be followed by UV/vis spectroscopy. Therefore, colourless MOFs are prefered.

The resulting compounds were analysed with regard to successful embedment (Incorporation), Composition and photochromic as well as solvatochromic response (Effects). This ICE-principle is indispensable for an adequate characterization and understanding of the resulting hybrid SP–O@MOF composites. Based on our results of the SP–Nitro@MOF systems[10] (SP-Nitro: 1,3,3- trimethylindolino-6'-nitro-benzopyrylospiran) the SP–O@MOF composites were investigated focusing on the following aspects:

(a) photoswitching properties and type of photochromism,
(b) influence of the host matrix on the absorption properties as well as stabilization of the embedded guest, and
(c) reversibility of switching as well as fatigue resistance.

2.1. Embedment

The successful incorporation of SP–O into the host matrices MOF-5, MIL-68(In), and MIL-68(Ga) was confirmed by XRPD measurements (X-ray powder diffraction). The results are exemplarily described for SP–O@MOF-5 (**1**) in Figure 2 (for **2** and **3** see Figures S1 and S2, Supporting Information). For **1**, pronounced alterations of the peak intensities are found when compared to the pattern of unloaded MOF-5. Especially for the first and second peaks, a significant decrease respectively increase in intensity points to the successful incorporation of the dye molecule. Note: reflections at ~12°, ~15°, ~18°, and ~20° (2θ) belong to **1** as confirmed by a *Le Bail* fit (Table 1 and Figure S3, Supporting Information).

After the MOF's pores were loaded, the integrity of the MOF framework remained intact, as indicated by the almost unaltered reflection positions. Furthermore, the presence of

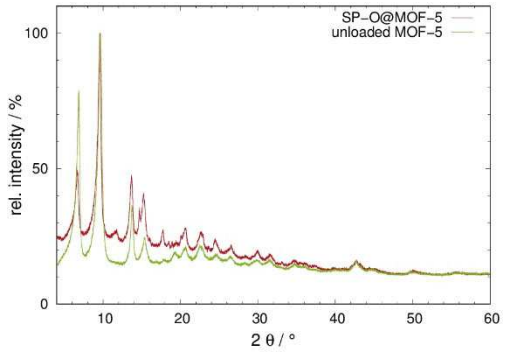

Figure 2. XRPD patterns of SP–O@MOF-5 (**1**, red) in comparison to unloaded MOF-5 (green), both measured at 298 K (*Huber G670*: $\lambda = 1.5406$ Å).

Table 1. Results of the *Le Bail* fits of X-ray powder diffraction data of **1** to **3**.

Parameters	1	2	3
T [K]	298	298	298
Space Grou /No.	$Fm\bar{3}m$/225	*Cmcm*/63	*Cmcm*/63
GOF	1.55	0.92	1.38
R_p	0.0310	0.0202	0.0276
wR_p	0.0469	0.0315	0.0431
V [Å^3]	16502(3)	5949(1)	5073(1)
a [Å]	25.459(5)	22.425(2)	20.546(3)
b [Å]	a	37.160(4)	37.594(6)
c [Å]	a	7.1388(7)	6.568(1)

free SP–O can be excluded since no additional peaks occur. Hybrid systems with MIL-68(In) and MIL-68(Ga) containing SP-O exhibit a behaviour very similar to the analogous compounds with the nitro-substituted spiropyran (SP-Nitro):[10] A pronounced gain in intensity of the third peak and loss in intensity of the first one indicate the successful embedment of SP–O for SP–O@MIL-68(In) (**2**) and SP–O@MIL–68(Ga) (**3**), cp. Figures S1 and S2 in the Supporting Information. Again, *Le Bail* fits using *JANA2006*[54] were used to confirm the purity of these two compounds (Figures S4 and S5 in the Supporting Information). The results of these *Le Bail* fits are further summarized in Table 1.

To corroborate the findings of the XRPD measurements and to confirm that SP–O is indeed embedded into the pores of the respective MOF hosts, N_2 sorption measurements were conducted on the pristine MOFs as well as loaded **1** to **3** (Figure S7, Supporting Information). To obtain comparable results, the same conditions for activation were used for the loaded and pristine samples (295 K, $1 \cdot 10^{-7}$ mbar, 4 h). The drastic decrease of the specific surface areas (S_{BET}) from 1467 to 237 m^2/g (MOF-5, **1**), 1629 to 45 m^2/g (MIL-68(In), **2**), and 483 to 36 m^2/g (MIL-68(Ga), **3**) clearly confirms the successful loading of the MOF hosts with SP–O guests. According to these measurements, the loading in both MIL-68 samples seems to be denser than in MOF-5. It should be noted that the specific surface areas of the pristine MOFs are different to those described on page S2 (Supporting Information), as different conditions for activation were used.

For the flexible MOF MIL-53(Al), a different behaviour is observed when combined with SP–O. Similar to the results obtained upon loading of SP-Nitro into MIL-53(Al),[10] the diffraction pattern remains unaltered with respect to intensity and position of the reflections in comparison to the unloaded MOF host (see Figure S6, Supporting Information), although a significant change of the diffraction pattern is expected upon guest loading due to the "breathing effect" of MIL-53(Al).[53] For SP-Nitro@MIL-53(Al), further spectroscopic measurements confirmed that the dye molecule is adsorbed as an amorphous film on the MOF surface,[10] which is also assumed for SP–O@MIL-53 (Al) (**4**). Although SP-Nitro was only adsorbed on the surface of MIL-53(Al), photochromic and solvatochromic response was observed for this hybrid material as well.[10] Therefore, we performed further investigations on the photoswitching properties of the SP–O/MIL-53(Al) system.

2.2. Composition (Degree of Loading)

The compositions of the SP-O@MOF composite materials were determined by means of XPS measurements. To this end, the areas of nitrogen core level signals were related to the areas of the metal cation signals of the respective MOF hosts (Zn, In, Ga, Al). The SP–O molecule contains two nitrogen atoms in its structure, which can be treated as electronically equal. Thus, only one N1s peak is expected for an isolated or surface adsorbed randomly oriented SP–O molecule, whereas peak broadening or even splitting is expected when being loaded into the MOF scaffold with a specific orientation. The results of the XPS measurements with respect to the composition of the switch@MOF materials under investigation are summarized in Table 2. The respective peak fits of the XPS data and more details of the quantitative analysis of these data are given in Figures 3, 4, S8 to S11, and Table S1, Supporting Information. It should be stated that XPS is a surface method. Hence, the composition of the surface with a penetration depth of approx. 10 nm is analysed. Therefore, additional DSC/TGA measurements were performed for comparison, which give insights into the composition of the bulk material (vide infra).

The comparison of typical nitrogen peaks of SP–O in MOF-5 (Figure S8, Supporting Information), MIL-68(In) (Figure 4), MIL-68(Ga) (Figure S10, Supporting Information) and MIL-53(Al) (Figure 3) reveals differences in the incorporation of the guest.

For SP–O combined with MIL-53(Al), only one peak is observed at approx. 399 eV, showing that both nitrogen atoms remain electronically equal. On the contrary, a slight peak splitting occurs for SP–O embedded in all other MOFs. The

Table 2. Ratio of SP–O per formula unit of the respective MOF for **1** to **4** calculated from XPS measurements.

Material		SP–O : MOF ratio
SP-O$_x$@MOF-5 (**1**)	SP–O : ($Zn_4O(bdc)_3$)	2.15 : 1
SP-O$_x$@MIL-68(In) (**2**)	SP–O : (In(OH)(bdc))	0.19 : 1
SP-O$_x$@MIL-68(Ga) (**3**)	SP–O : (Ga(OH)(bdc))	0.29 : 1
SP-O$_x$@MIL-53(Al) (**4**)	SP–O:(Al(OH)(bdc))	0.13 : 1

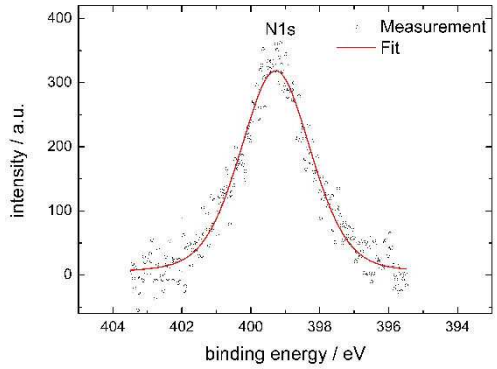

Figure 3. XPS spectrum of SP–O@MIL-53(Al) (**4**) showing the region of the N1s peak with experimental data (grey dots) and fit to the data (red curve).

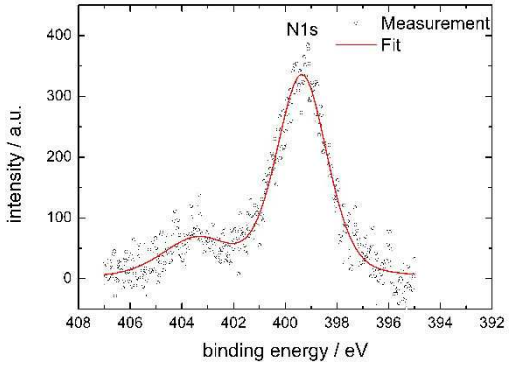

Figure 4. XPS spectrum of SP–O@MIL-68(In) (**2**) showing the region of the N1s peak with experimental data (grey dots) and fit to the data (red curve).

nitrogen N1s peak area is exemplarily shown for SP-O@MIL-68 (In) (**2**) in Figure 4. In addition to the most intensive peak at 399 eV, a second one at approx. 404 eV appears, which is not present in **4**, but in **1** and **3** as well (Figures S8 and S10, Supporting Information). This confirms an embedment of SP–O with a specific orientation in the pores of the MOFs in **1** to **3**, whereas in **4** only surface bound SP–O with a random orientation is found.

For SP–O embedded in MOF-5 (**1**), the XPS measurements result in a SP–O:MOF ratio of 2.15:1 (Table 2), which means that on average each of the two differently sized cavities contains approx. two SP–O molecules. For MOFs of the MIL series with channel-like pores, such an assignment is not possible. It should be emphasized that the ratios given in Table 2 refer to one metal for **2** to **4** and four metals for **1**. Nonetheless, the filling of the pores in MOF-5 seems to be significantly higher than in the other MOF hosts, obviously due to the higher porosity of MOF-5 (for details on pore sizes and BET surface areas of the used MOFs see page S2, Supporting Information). Furthermore, for MIL-68 only the hexagonal channels are large enough to accommodate the SP–O guest molecules so that the trigonal channels are assumed to remain unfilled. For MIL-53 it was already concluded that no filling of the pores with SP–O occurred and SP–O molecules are only adsorbed on the surfaces of the MOF particles. This finding is in agreement with the low SP–O:MOF ratio found for **4** (Table 2).

In addition to the composition analyses via XPS, DSC/TGA measurements were performed under an argon atmosphere. For MOF-5 as host material, one endothermic signal is present in the DSC curve (red line) at 150 °C without a corresponding mass loss (see Figure 5). This endothermic signal is attributed to the thermal repopulation of the closed SP–O form of the spirooxazine. At higher temperatures, two mass losses without corresponding exo- or endothermic signals are found (blue line). The first mass loss starts at approx. 170 °C (mass loss: ~38%) and the second one at approx. 400 °C (mass loss: ~32%). As these two effects almost continuously merge into each other, a clear quantitative assignment is difficult.

Assuming the composition as obtained from XPS measurements, a mass loss of 48% is expected. This value is reached at approx. 400 °C. Above that temperature, the decomposition of the MOF framework starts leading to a remaining mass of ~28% (22% calculated for ZnO). Hence, in general the DSC/TGA investigations confirm the composition of **1** as obtained from XPS data. To corroborate this interpretation in Figure S15 (a) (Supporting Information), the TGA data of **1**, activated MOF-5 and pristine SP–O measured under the same conditions are compared. Starting at approx. 200 °C SP–O is released, which is close to the sublimation temperature of the pristine compound. The decomposition temperature of MOF-5, which was given as ~450 °C,[55] is slightly decreased in the loaded compound **1** to ~420 °C. As this is found for all MOF hosts (Figure S15), loading with SP–O obviously seems to decrease the thermal stability of the respective MOF. Interestingly, between ~300-400 °C a slower release of guest molecules is observed. As will be shown later (cp. Figure 6), in MOF-5 SP–O already exists to a larger extent in its coloured merocyanine form without UV light exposure. As this isomer shows a higher polarity compared to its spiro form, a stronger interaction with the highly charged $[Zn_4O]^{6+}$ nodes can be assumed leading to an enhanced releasing temperature. Obviously, the strong interaction with the $[Zn_4O]^{6+}$ nodes hinders the repopulation of the spiro ground state upon heating (see endothermic signal at ~150 °C), which is only possible for SP–O (MC–O) molecules weakly

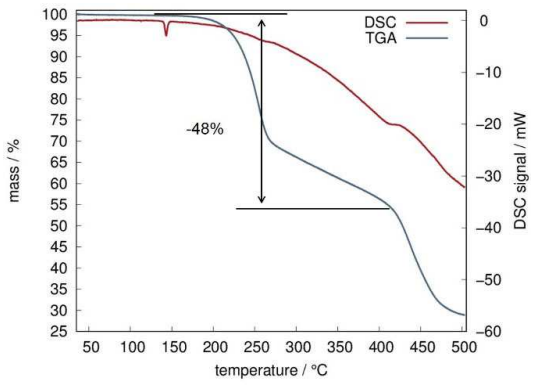

Figure 5. DSC/TGA measurements of SP–O@MOF-5 (**1**) under an argon atmosphere in the range of 30 to 500 °C. The DSC curve is shown in red, the TGA curve in blue.

Figure 6. **1** to **4** before (left) and after (right) irradiation with UV light ($\lambda = 365$ nm, 1 min, right).

bound to the MOF host, i.e. oriented towards the linker or mobile in the inner part of the pore. In future experiments, we are planning to clarify this surely interesting behaviour by solid-state NMR experiments.

A different thermal behaviour is observed for materials with MIL-68(In) and MIL-68(Ga) as hosts. For both (**2** and **3**), no endo- or exothermic signals are found below 400 °C in the DSC curves (see Figures S12 and S13, Supporting Information), which is in agreement with the finding (vide infra) that in both MOF hosts SP–O is only embedded in its spiro form. Starting at temperatures of approx. 160 °C, a continuous mass loss is observed for both SP–O@MIL-68 materials. Obviously, the release of guest molecules and the decomposition of the MOF host overlap making a precise quantitative analysis difficult. In Figure S15(b,c) (Supporting Information), the TGA curves of **2** resp. **3**, pristine SP–O, and the respective activated MOF host are compared. The decomposition temperatures of MIL-68(In) and MIL-68(Ga), which were given as 340 °C in the literature,[52] are found at significantly higher temperatures (> 400 °C). However, for the SP–O loaded compounds **2** and **3** this decomposition temperature is slightly shifted to lower temperatures, as already found for **1** compared to activated MOF-5 (vide supra). Assuming the composition as obtained from XPS data (see Table 2), a mass loss of 17.4 % for **2** and 27.5 % for **3** is expected. These values are reached, when the decomposition of the MOF host starts (~ −19 % for **2** and ~ −26 % for **3**). In general, the results of the DSC/TGA investigations corroborate the findings of the XPS data, but as the release and the decomposition of the MOF framework overlap, a precise analysis is difficult and a rough estimate can only be obtained by comparing DTA data of the loaded samples SP–O@MOF with those of the empty MOF and the pristine SP–O guest.

As a third method to determine guest:host ratios, we used solution ^{1}H NMR experiments, i.e. the host is decomposed by an acid (DCl) and in the resulting DMSO-d_6 solution the proton signals of the MOF linker (here: terephthalic acid) and the guest (here: SP–O) are integrated to obtain the desired ratios.[9] During our experiments we found that DCl does not only decompose the MOF framework, but also SP–O is protonated and starts to decompose.[56–58] In "fast" (5 min after addition of DCl) NMR experiments on compounds **1**, **2** and **3** (Figure S16, S17 and S18, Supporting Information) we observed SP–O:MOF ratios of 0.99:1 (**1**), 0.15:1 (**2**) and 0.20:1 (**3**), which are, for **2** and **3**, in reasonable agreement with those obtained from XPS measurements (Table 2) showing that the latter is an elegant, non-destructive way to analyse such systems quantitatively. Using the solution NMR approach, we did not obtain meaningful results for **1** and **4**. For **1**, the obtained ratio differs to a higher extent to the result of the XPS measurements (Table 2), which might be a consequence of the above mentioned SP–O decomposition under acid conditions. For **4**, no complete decomposition of the MIL-53(Al) framework was achieved. Replacing DCl by HF showed that SP–O is more stable after addition of this weaker acid, but residual powder remained at the bottom of the NMR tube indicating a non-complete decomposition of the MOF framework.

From XRPD and XPS data it was concluded that SP–O is not embedded in the pores of MIL-53(Al), the MOF host with the smallest channels (page S2, Supporting Information). Instead, an adsorption of SP–O molecules on the surfaces of MIL-53(Al) particles was assumed (vide supra). The resulting DSC/TGA curves are presented in Figure S14 (Supporting Information). The DSC curve does not show any significant signal between room temperature and 500 °C with the exception of a tiny endothermic signal at 150 °C, which might indicate a very minor amount of SP–O in its merocyanine form (see the very light green colour of **4** before exposure to UV light in Figure 6) that is back-switched to its spiro form upon heating. The TGA curve shows two distinct steps with mass losses of 5.5 % (up to ~ 270 °C) and 10.5 % (up to 500 °C). The first step correlates nicely with the sublimation temperature of pristine SP–O (Figure S15(d), Supporting Information). As known from literature, MIL-53(Al) decomposes above 500 °C,[50] which is higher than the temperature range of our investigations. From the XPS data a release of surface-adsorbed SP–O molecules of approx. 17 mass-% is calculated, which is in reasonable agreement with the sum of both mass losses (5.5 % + 10.5 %). But it is unclear at the moment, why two distinct steps are observed. The occurrence of larger amounts of SP–O molecules in its merocyanine form, as observed for **1**, can be excluded, as explained above.

2.3. Photoswitching and Type of Photochromism

To investigate the light induced isomerization processes and to determine the type of photochromism, UV/vis absorbance spectra before and after irradiation with UV light ($\lambda = 365$ nm, 30 min) of all compounds **1** to **4** were recorded under inert conditions. Switching of pure SP–O is only possible, when deposited as thin films,[59,60] in single-crystalline phase at very low temperatures[61] or by irradiation with intense UV light (high pressure Hg lamp).[62] Here, photoswitching of SP–O embedded into the different MOF frameworks was achieved by a common UV lamp at room temperature. Under these conditions, photoswitching of SP–O has not been observed before in the solid state. To corroborate this, we illuminated pure SP–O and SP–O@MIL-68(In) (**2**) under the same conditions with UV light ($\lambda = 365$ nm, 1 min). While a significant colour change was observed for **2**, no photoresponse was found for the pristine SP–O under these conditions (Figure S19, Supporting Information). This clearly shows that embedment of SP–O

into a porous MOF improves its photoswitching properties significantly.

The change in colour upon UV light irradiation is depicted in Figure 6 indicating that the embedment of SP–O into MOF-5 already causes stabilization of the strongly coloured merocyanine form, which has also been observed for SP-Nitro embedded in MOF-5.[10] For SP-O embedded in MIL-68(Ga/In) the coloured MC–O isomer is only formed upon UV light exposure. For SP–O adsorbed on the MIL-53(Al) surface (**4**), the very light green colour points to very minor amounts of MC–O in this system. We ascribe the formation of green-coloured SP–O in its open merocyanine form in MOF-5 (also cp. Figure 7, blue curve) to the high polarity within these pores, which are built from highly charged $[Zn_4O]^{6+}$ nodes. The latter are expected to stabilize the polar merocyanine form better than the pores of MIL-68 with a lower polarity. A similar finding was reported for spiropyran embedded in JUC-120, an analogue of MIL-100.[11]

In Figure 7, the absorbance spectra of **1** before and after UV light irradiation are shown (for **2** and **3**: see Figures S20 and S21, Supporting Information). A small peak at $\lambda = 631$ nm is already present without irradiation (vide supra), which can be clearly attributed to the presence of SP–O in its open merocyanine form (blue line). UV light exposure results in further strengthening of this absorption maximum at $\lambda =$ 631 nm with a blue-shifted shoulder at approx. 580 nm (red line) indicating the proceeding formation of the merocyanine moiety upon excitation. The asymmetric shape of the MC–O's absorption band is well known.[33] Hence, the polar merocyanine form is stabilized within the pores of MOF-5 pointing to an environment of these cavities, which is preferred by molecules with high dipole moments such as merocyanines. Additionally, positive photochromism takes place, since an absorption maximum is formed upon UV light irradiation.

This positive photochromism is also found for **2** and **3** (Figures S20 and S21, Supporting Information). For both composite materials only a very weak peak is observed before irradiation with UV light, which does not lead to a coloured product (Figure 6). The formation of the coloured MC–O can be followed by the light induced appearance of a strong absorption band at 629 nm (**2**) and 624 nm (**3**), respectively.

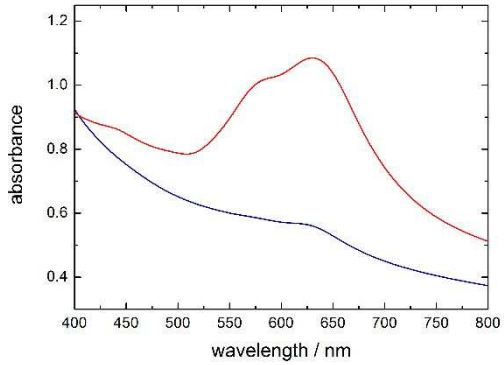

Figure 7. Absorbance spectra (298 K) of SP–O@MOF-5 (**1**) before (blue) and after (red) irradiation with UV light ($\lambda = 365$ nm, 30 min).

Moreover, blue-shifted shoulders occur as well, which are positioned at 577 nm (**2**) and 575 nm (**3**). When compared to **1**, both absorption maxima are slightly blue-shifted in **2** and **3**. Importantly, for all compounds **1** to **3** the light induced switching processes are obviously not sterically hindered inside the MOF scaffold and a free and undisturbed photoswitching can occur.

Figure 8 depicts the absorbance spectra of non-irradiated (blue line) and irradiated (red line) SP–O/MIL-53(Al) (**4**). As already concluded from the XRPD and XPS measurements, surface adsorption of the dye molecule occurs in this material.

Nevertheless, the combination of SP–O with MIL-53(Al) exhibits photochromic behaviour with an absorption maximum at approx. 613 nm, which is significantly blue-shifted in comparison to the other SP–O@MOF systems. Furthermore, a small shoulder appears at around 566 nm.

Further investigations were done by means of IR spectroscopy to understand and prove the SP–O to MC–O conversion, both before and after irradiation with UV light. The conversion of SP–O to its MC–O form results in the cleavage of the C_{spiro}-O bond. Therefore, the decrease of this band at approx. $\tilde{\nu} =$ 965 cm^{-1} was used to track the formation of MC–O.[63] For **1**, the spectra in this region are shown in Figure 9. A significant decrease of the C_{spiro}–O band was observed with increasing UV

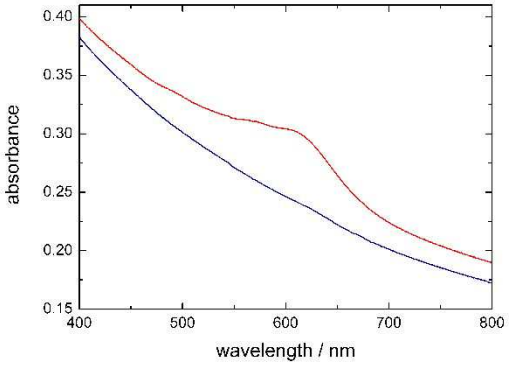

Figure 8. Absorbance spectra (298 K) of SP–O@MIL-53(Al) (**4**) before (blue) and after (red) irradiation with UV light ($\lambda = 365$ nm, 30 min).

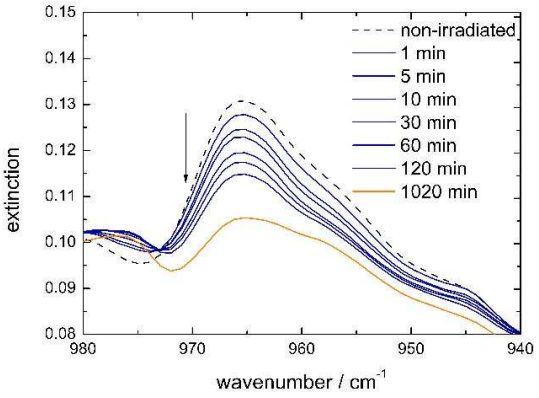

Figure 9. IR spectra of **1** during irradiation with UV light ($\lambda = 365$ nm) focusing on the decrease of the C_{spiro}-O band at approx. $\tilde{\nu} = 965$ cm^{-1}; the direction of the decrease is marked with an arrow.

light exposure times, pointing to the successful formation of the excited MC–O form inside MOF-5. For the other MOFs, see chapter "Photostability and reversibility of switching".

2.4. Influence of the Host Matrices on the Absorption Properties

The open merocyanine form of SP–O (MC–O) exhibits positive solvatochromism with increasing solvent polarity. When embedded in the different host matrices MOF-5 and MIL-68(In/Ga) or when adsorbed on the surface of MIL-53(Al), the absorption bands are increasingly blue-shifted (cp. Table 3). By taking the positive solvatochromism of MC–O into account, MOF-5 represents the most polar and the surface of MIL-53(Al) the least polar host matrix, analogous to previously reported results on SP-Nitro.[10] Incorporation of SP–O into MOF-5 already causes a stabilization of MC–O in the absence of UV light. To understand this response of MC–O, the structures of the SP–O@MOF composites need to be studied in more detail. In all compounds, the same bdc^{2-} linker is used in the MOF hosts so that alterations in the absorption behaviour must be related to the inorganic nodes – $[Zn_4O]^{6+}$ for MOF-5 and $[InOH]^{2+}$/$[GaOH]^{2+}$ for MIL-68(In)/MIL-68(Ga) – and/or the size and shape of the pores. Simply looking at the charges of the nodes the higher polarity within the MOF-5 pores is not surprising due to the high charge of the $[Zn_4O]^{6+}$ node. For MIL-53(Al) with $[AlOH]^{2+}$ units, a higher polarity than for MIL-68(In/Ga) with $[In/GaOH]^{2+}$ units is expected due to the smaller ionic radius of Al^{3+}. As this is not observed – with MIL-53(Al) the strongest hypsochromic shift is found –, this may be interpreted as the final hint that SP–O is not embedded in the pores of this MOF, but on its surface. The successful isomerization of SP–O to MC–O and the influence of the host matrix on its absorption behaviour strongly resemble the properties of spirooxazine dissolved in solvents of varying polarity. Thus, MOFs can be considered as "solid solvents" not only for spiropyrans,[10] but also for the structurally related spirooxazines.

As already mentioned earlier, a blue-shifted shoulder is found in the absorbance spectra of all compounds **1** to **4**. For spirooxazines the appearance of asymmetric absorption maxima with batho- or hypsochromically shifted shoulders is well-known.[33] Therefore, in Table 3 a mean value $\lambda_{average}$ is given, as the local absorption maximum and the respective shoulder cannot be considered as isolated signals.

Table 3. Absorption maxima of SP–O@MOF after irradiation with UV light ($\lambda = 365$ nm); $\lambda_{average}$ is the mean value of λ_{max} and $\lambda_{shoulder}$.

	λ_{max} [nm]	$\lambda_{shoulder}$ [nm]	$\lambda_{average}$ [nm]
SP–O@MOF-5 (**1**)	631	580	605.5
SP–O@MIL-68(In) (**2**)	629	577	603.0
SP–O@MIL-68(Ga) (**3**)	624	575	599.5
SP–O/MIL-53(Al) (**4**)	613	566	589.5

2.5. Photostability and Reversibility of Switching

By IR and UV/vis spectroscopic measurements, the photostability and the fatigue resistance of the SP–O@MOF composite materials were studied. Upon irradiation with UV light, the IR bands of the SP–O form decrease, while the ones of the MC–O form increase, which can be easily tracked in the IR spectra, as shown for the C_{spiro}–O band in **1** (Figure 9). An exact assignment of all IR bands to the respective isomer (SP–O and MC–O, respectively) was performed for SP–O@MOF-5. Following the work of *Lyubimov* and co-workers[64] and *Paal* and *Arnold*,[63] the decreasing IR bands of the SP–O form were completely assigned for this system.

To facilitate this assignment, the spectrum of non-irradiated **1** was subtracted from the spectra of UV-irradiated **1** with different irradiation times to obtain ext_{irrad}-$ext_{ground\ state}$. The resulting (difference) spectra of **1** are depicted in Figure 10 with changing bands coloured in blue and the difference signal for maximal irradiation coloured in orange. As the open MC–O forms upon UV light irradiation, all bands above zero are increasing IR bands, which belong to the excited form, whereas all bands beyond zero can be assigned to the closed SP–O form, which depopulates during the UV light irradiation process.

Notably, largest changes are found for the longest irradiation time, which shows that no photodegradation at least up to an irradiation time of 720 min takes place. Hence, increasing IR bands in these plots can be fully assigned to the merocyanine moiety, which has not been done in the literature so far to the best of our knowledge.

In Table S2 in the Supporting Information, the decreasing vibrational frequencies of SP–O@MOF-5 (**1**) and their assignments according to the literature[63,65] are listed. For a better understanding, the structures of the closed SP–O and open TTC form (the most stable isomer of MC–O according to quantum chemical calculations[66,67]) are depicted in Figure 11, in which the different rings are labelled. All decreasing vibrational frequencies were completely assigned to the closed form of SP–O, which confirms the successful isomerization of SP–O to its open MC–O form. Moreover, increasing IR bands of **1** were

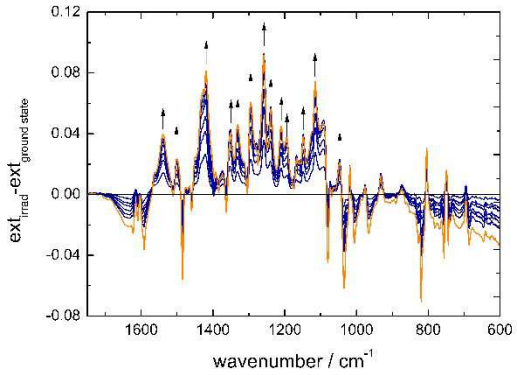

Figure 10. Difference IR spectra of SP–O@MOF-5 (**1**). The spectrum for the longest irradiation time (720 min) is coloured in orange; the direction of increasing bands is marked with arrows.

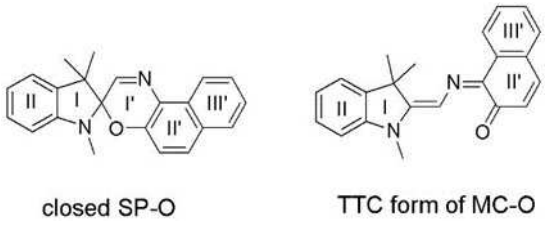

Figure 11. Comparison of SP–O in its closed form and the TTC form of the respective merocyanine.

also analysed. The assignments for the irradiated species are given in Table S3 (Supporting Information) according to *Lyubimov* and co-workers[64] and *Paal* and *Arnold*.[63]

The unassigned vibrational frequencies were allocated according to a common textbook on spectroscopy.[65] To facilitate these assignments, the TTC mesomeric form of the merocyanine moiety of SP–O was examined more precisely with respect to changing bonds in comparison to closed SP–O (Figure 11). While the rings I, II and III′ remain unaffected by the light induced cleavage of the C_{spiro}–O bond, ring I′ is completely destroyed and II′ changes structurally. That way, all increasing bands were attributed to the respective vibrational modes, again pointing to a successful SP–O to MC–O conversion without the formation of any photo-by-product (Table S3, Supporting Information). Obviously, the photostability of SP–O remains unaffected by the incorporation into MOF-5.

Additionally, we recorded UV/vis spectra of **1** after different irradiation times with UV light ($\lambda = 365$ nm, 1–30 min, Figure 12). For a better visualization of the occurring processes, the absorption of the non-irradiated species was subtracted from the absorption of the irradiated samples. In contrast to compounds **2** to **4** (Figures S22 to S24, Supporting Information), the intensity of the absorption band at $\lambda = 631$ nm increases constantly upon UV light exposure, pointing to a high photostability of SP–O inside the MOF-5 matrix, which corroborates the results of the IR spectroscopic measurements. Moreover, a shoulder at approx. $\lambda = 480$ nm appears, which has not been seen so far, but is also observed for **2** and **3** for

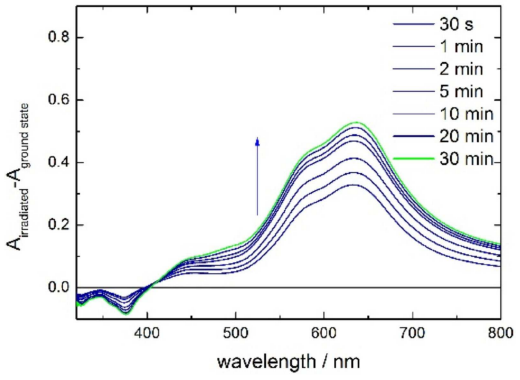

Figure 12. Difference UV/Vis spectra of SP–O@MOF-5 (**1**) for prolonged UV light irradiation ($\lambda = 365$ nm, 1–30 min); the direction of the increase is marked with an arrow.

prolonged UV irradiation times (Figures S22 and S23, Supporting Information). We assume that aggregation processes take place, but this needs to be further confirmed by additional methods like solid state NMR spectroscopy.

In contrast to MOF-5 as host material, the intensity of the characteristic absorption band of MC–O decreases upon prolonged UV light exposure, when embedded or combined with hosts of the MIL family (Figures S22 to S24, Supporting Information). Although SP–O exhibits a remarkable photostability, the surrounding host matrix influences the fatigue resistance significantly. MOF-5 stabilizes the electronic structure in a way that photo-by-products are not produced even upon prolonged UV light exposure, whereas with other host materials no such photostabilization was found. In order to understand this behaviour in more detail, it is necessary to include quantum-chemical calculations in further investigations.

In a next step, we performed irradiation experiments to investigate the reversibility of switching of the four hybrid systems. Both, UV/vis and IR spectroscopic measurements were applied and will be exemplarily discussed for MOF-5 and MIL-53(Al) as host materials. Repopulation was triggered by both thermal and photochemical treatment. In order to start from the "real" ground state, the hybrid materials SP–O@MOF-5 (**1**) and SP–O@MIL-53(Al) (**4**) were irradiated with visible light ($\lambda = 625$ nm). In both cases, the small absorption maximum in the UV/vis spectra disappears (see Figures S25 and S26 in the Supporting Information for **1** and **4**). Subsequent irradiation with UV light triggers the formation of the coloured merocyanine form, which can be reversibly reconverted to the spirooxazine form by thermal treatment (room temperature for several minutes) or by photochemical means, see Figure 13 top/bottom for **1**. For MIL-53(Al), surface adsorption of the dye molecule allows reversible photoswitching in the solid state with no significant fatigue after three switching cycles (see Figure 14, bottom). Here, depopulation of the merocyanine form is induced via irradiation with visible light with $\lambda = 625$ nm. In Figure 14, top, the UV/vis spectra of three switching cycles are depicted. Formation of the MC–O form is induced by UV light, whereas reconversion to the ground state is reached by visible light irradiation. By looking at the IR spectra of **1** to **4**, photochemical relaxation to the ground state is much more efficient than thermal treatment (see Figures S27 to S29 in the Supporting Information).

For excited SP–O@MOF-5 (**1**), 1 min of visible light irradiation causes a more efficient depopulation into the ground state than 60 min thermal treatment at room temperature, where only small repopulation occurs (see Figure 15 top and bottom). In contrast to that, 60 min at room temperature cause significant reconversion to the ground state for MIL-68(In) and MIL-68(Ga) as host materials (see Figures S27 and S28 in the Supporting Information).

However, only 40 min at room temperature are enough for a nearly complete reconversion of MC–O to SP–O on the surface of MIL-53(Al) (see Figure S29 in the Supporting Information). Obviously, MC–O is thermally stabilized inside or on the surface of the different MOF hosts, but the thermal

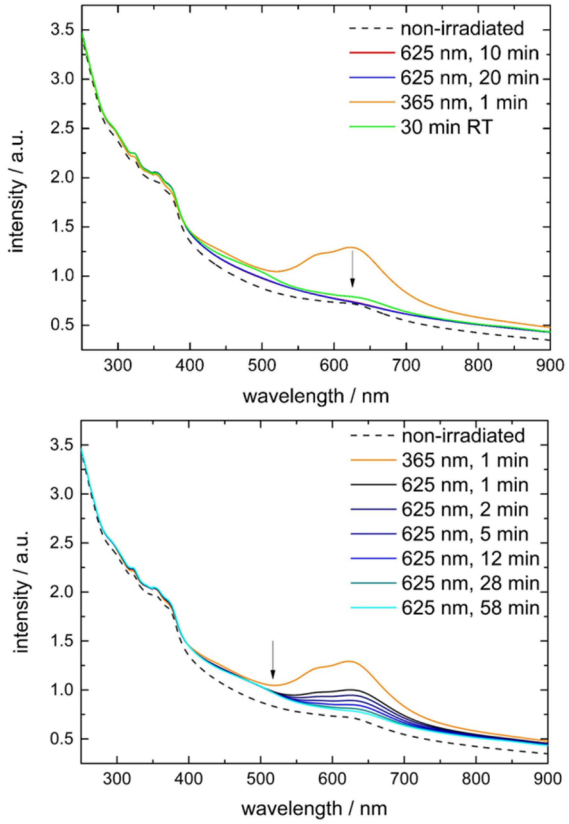

Figure 13. UV/Vis absorption spectra of both thermal and photochemical (top) and purely photochemical (bottom) relaxation of SP–O@MOF-5 (**1**) after UV light irradiation for 1 min.

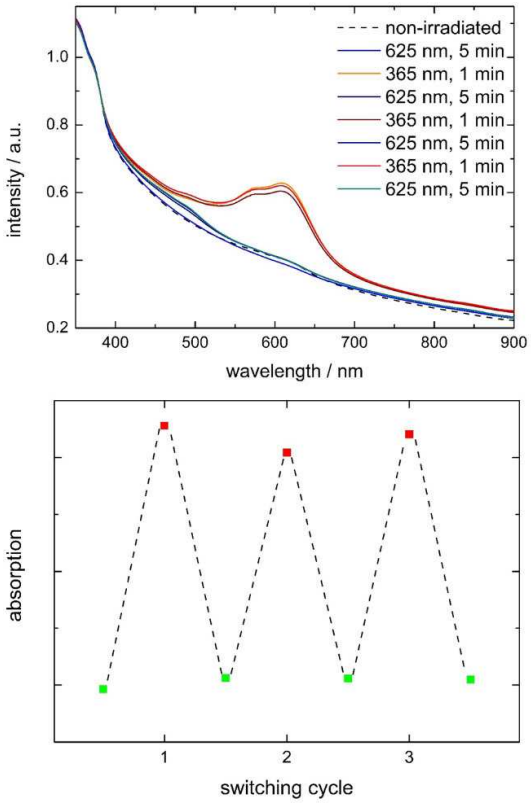

Figure 14. UV/Vis absorption spectra of three switching cycles, induced by photochemical treatment (top) of SP–O@MIL-53(Al) (**4**); bottom: visualization of the switching cycles with no significant fatigue visible after three cycles.

stabilization depends on the type of the MOF scaffold. In order to understand the different stabilization processes, the position of the spirooxazine molecules inside the MOF pores has to be determined, which is currently under way.

3. Conclusions

We herein presented the first spirooxazine@MOF composite materials with SP–O (1,3,3-trimethylindolinonaphtho-spirooxazine) as a non-covalently attached guest molecule. SP–O was combined with the four host matrices MOF-5, MIL-68(In), MIL-68(Ga), and MIL-53(Al). While it was clearly proven that SP–O is embedded in MOF-5, MIL-68(In), and MIL-68(Ga), only surface adsorption occurs for MIL-53(Al). Noteworthy, the latter exhibits the smallest pores of all four MOFs.

Nevertheless, all four composite materials exhibit a photochromic as well solvatochromic response, which is similar to the dissolved state of the dye molecule and strengthens the concept of MOFs as "solid solvents" for photoactive dye molecules, which has been reported before.[10]

The switching processes were tracked by UV/vis and IR spectroscopy for all compounds. IR bands of the non-irradiated species were completely assigned to the closed form of the spirooxazine. Moreover, vibrational frequencies of the excited species were determined and assigned, which has, to the best of our knowledge, not been reported before, so that we also present the first IR spectroscopic data of the open MC–O form of the studied spirooxazine.

In agreement with the results on SP-Nitro (1,3,3- trimethylindolino-6'-nitro-benzopyrylospiran) embedded in MOF-5,[10] SP-O is present in its open merocyanine form in MOF-5 as well. But most importantly, photodegradation of SP–O is completely suppressed in MOF-5 even upon prolonged UV light exposure (up to 720 min) but was found to occur in MIL-68(In), MIL-68 (Ga), and on MIL-53(Al). However, short irradiation times were found to cause no fatigue for SP-O@MIL-53(Al). For all investigated hybrid systems, reconversion to the ground state was found to be most efficient by photochemical means.

In summary, the obtained guest@MOF composite materials are of great importance for understanding the influence of the host material on the photochromic and solvatochromic properties of the embedded guest molecules. Successful photoswitching as well as a significant solvatochromic response was observed for all four SP-O@MOF materials. Nonetheless, determination of the exact position of the incorporated guest molecules inside the MOF pores is obligatory to understand the light induced response in more detail. However, structure solution, even via high resolution synchrotron powder diffraction, is difficult, since the embedded dye molecules are, in contrast to e.g. azobenzene,[4] too complex for such investigations. Furthermore, within MOF-5 with a high cubic symmetry a strong disorder complicates the interpretation of

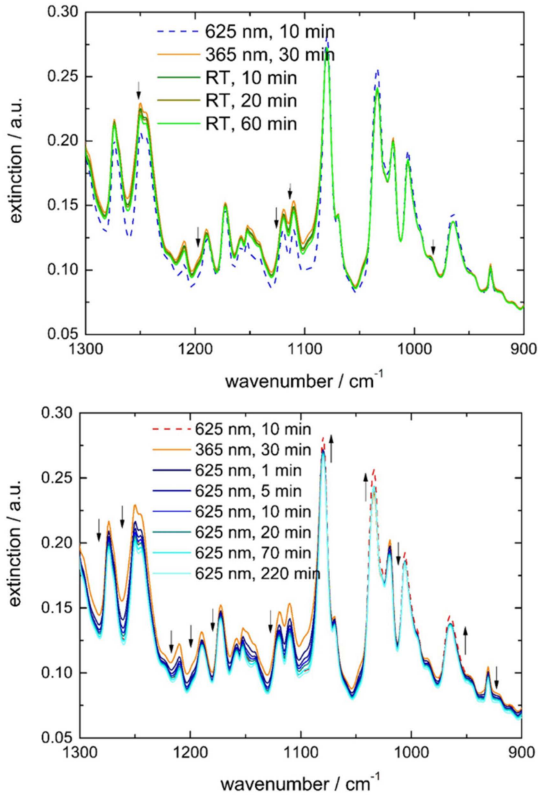

Figure 15. Comparison of both thermal and photochemical (top) and purely photochemical (bottom) relaxation to the ground state of SP–O@MOF-5 (**1**) followed by IR spectroscopy.

such data. Therefore, in a next step, complementary methods such as solid-state NMR spectroscopy and PDF (pair distribution function) analysis in combination with quantum-chemical calculations will be applied to obtain a reliable determination of the dye position within the MOF pores.

Experimental Section

1,3,3-Trimethylindolinonaphthospirooxazine ($C_{22}H_{20}N_2O$, SP-O). SP-O was used as purchased (TCI) without further purification.

Syntheses of the Host Materials

All host materials were synthesized according to the literature known procedures. Commercially available *N,N'*-dimethyl formamide, DMF (Acros Organics), $Ga(NO_3)_3 \cdot xH_2O$ (ABCR), $In(NO_3)_3 \cdot 5H_2O$ (ABCR), $Al(NO_3)_3 \cdot 9H_2O$ (ABCR), triethylamine, $Zn(OAc)_2 \cdot 2H_2O$, chloroform (Alfa Aesar) and terephthalic acid (Alfa Aesar) were used without further purification.

MOF-5. MOF-5 was synthesized following the protocol given in the literature.[68] 1.266 g terephthalic acid (7.62 mmol) and triethylamine (2.13 ml) were dissolved in 100 ml of DMF. 4.25 g $Zn(OAc)_2 \cdot 2H_2O$ (19.35 mmol) was dissolved in 125 ml DMF. While stirring, the zinc salt solution was added dropwise to the organic solution over 15 min. The mixture was stirred for 2.5 h. The precipitate was filtered off and immersed in 62.5 ml DMF overnight. It was then filtered off again and immersed in 87.5 ml $CHCl_3$. The solvent was exchanged 3 times over 7 days. Finally, the precipitate was decanted. To remove the solvent completely, the resulting powder was heated at 100 °C for 12 h under reduced pressure and stored under an argon atmosphere in the glovebox to prevent absorption of humidity and decomposition by contact with moisture. The phase purity was confirmed by XRPD.

MIL-68(Ga) ($GaOH(C_8H_4O_4) \cdot 0.9DMF \cdot zH_2O$) and MIL-68(In) ($InOH(C_8H_4O_4) \cdot 1.0DMF \cdot zH_2O$). MIL-68(Ga) and MIL-68(In) were synthesized by following mainly the protocol given in the literature.[52]

For MIL-68(In) 408.20 mg $In(NO_3)_3 \cdot 5\ H_2O$ (1.04 mmol) and 200.00 mg terephthalic acid (1.20 mmol) were mixed with 5.0 ml DMF in a 23 ml Teflon lined autoclave. The mixture was heated to 100 °C with a rate of 20 °C/h, kept at this temperature for 48 h, and afterwards cooled down to room temperature with a rate of 5 °C/h. The resulting colourless powder was washed several times with DMF and dried in air. To remove the embedded DMF molecules, the powder was heated in air at 200 °C for 12 h, then at 100 °C for 1 h under reduced pressure and was stored afterwards under an argon atmosphere in the glovebox to prevent absorption of humidity. The phase purity was confirmed by XRPD.

For MIL-68(Ga) 207.40 mg $Ga(NO_3)_3 \cdot xH_2O$ (0.81 mmol) and 100.00 mg terephthalic acid (0.60 mmol) were mixed with 5.0 ml DMF in a 23 ml Teflon lined autoclave. The mixture was heated to 100 °C with a rate of 20 °C/h, kept at this temperature for 48 h, and afterwards cooled down to room temperature with a rate of 5 °C/h. The resulting colourless powder was washed several times with DMF and dried in air. To remove the embedded DMF molecules, the residue was heated in air at 200 °C for 12 h, then at 100 °C for 1 h under reduced pressure and was stored under an argon atmosphere in the glovebox to prevent absorption of humidity. The phase purity was confirmed by XRPD.

MIL-53(Al) ($AlOH(C_8H_4O_4)$). MIL-53(Al) was synthesized according to the protocol known in the literature[53] with variations in the amount of the starting materials and the applied temperature programs. 1.95 g $Al(NO_3)_3 \cdot 9H_2O$ (5.20 mmol) and 432.00 mg of terephthalic acid (2.60 mmol) were mixed with 5.0 mL of deionized water in a 23 mL Teflon lined autoclave. The mixture was heated to 180 °C at 10 °C/h, kept at this temperature for 72 h, and afterwards cooled to room temperature at 5 °C/h. The resulting colourless powder was washed with deionized water several times and dried in air. To remove the embedded terephthalic acid molecules, the residue was heated in air at 350 °C for 7 days followed by 3 days of heating at 400 °C. Finally, the resulting powder was heated at 100 °C for 1 h under reduced pressure and stored under an argon atmosphere in the glovebox to prevent absorption of humidity. The phase purity was confirmed by XRPD.

Preparation of SP-O@MOF Systems

A mixture of the respective activated MOF and SP–O was ground thoroughly under an argon atmosphere. The resulting homogeneous powder was placed into a small glass vessel inside a Schlenk tube and heated at 145–150 °C and a reduced pressure of $\sim 5 \times 10^{-2}$ mbar for several hours. The excess of SP–O resublimed at the top of the glass tube. To prevent the absorption of water and decomposition upon contact with air and moisture, all compounds were stored in a glovebox under an argon atmosphere.

*SP-O_x@MOF-5 (**1**).* The synthesis was carried out as described above with 60.00 mg (0.08 mmol) MOF-5 and 128.5 mg (0.4 mmol) SP–O yielding a green powder.

*SP-O_x@MIL-68(In) (**2**).* The synthesis was carried out as described above with 60.00 mg (0.20 mmol) MIL-68(In) and 66.60 mg (0.20 mmol) SP–O yielding a colourless powder.

*SP-O_x@MIL-68(Ga) (**3**)*. The synthesis was carried out as described above with 60.00 mg (0.24 mmol) MIL-68(Ga) and 78.60 mg (0.24 mmol) SP–O yielding a colourless powder.

*SP-O_x@MIL-53(Al) (**4**)*. The synthesis was carried out as described above with 60.00 mg (0.28 mmol) MIL-53(Al) and 47.37 mg (0.28 mmol) SP–O yielding a colourless powder.

The purity of all resulting guest@MOF materials was checked by XRPD (Figure 2, Figures S1, S2, and S6, Supporting Information).

X-ray Powder Diffraction

To check the purity of the crystalline samples, laboratory measurements were carried out on a *Huber G670* powder diffractometer (Guinier geometry, Ge (111) monochromator, image plate detector) with Cu $K_{\alpha1}$ radiation. For each measurement, samples were prepared under an argon atmosphere to prevent absorption of humidity and decomposition. For that purpose, the respective MOF or hybrid system was thoroughly ground and filled about 2 cm high into *Lindemann* glass capillaries (diameter 0.7 to 1.0 mm). The filled capillaries were sealed with the help of a glow wire and closed airtight with picein wax. Data were collected at 298 K between 4 and 80.70° in 2θ with steps of 0.005° and a measurement time of 2 s/step.

Additionally, MIL-53(Al) *ht* was measured on a *STOE Stadi P* diffractometer (Ge monochromator, PSD detector) with Cu $K_{\alpha1}$ radiation. Data were collected at 298 K between 4° and 80.70° in 2θ with steps of 0.01° and a measurement time of 5 s/step. Seven such scans were added for one measurement.

N_2 Sorption

N_2 sorption measurements were carried out at 77 K with an AUTOSORB-1-MP instrument (Quantachrome). Prior to the sorption measurements, the sample was evacuated at room temperature for 4 hours ($1\cdot10^{-7}$ mbar). The Brunauer-Emmett-Teller (BET) surface area was calculated based on the pressure region $p/p_0 =$ 0.0005–0.03.

XPS

For XPS measurements, SP–O@MOF powders were placed on an adhesive copper foil. Measurements were performed on a multichamber UHV system at a pressure of 5×10^{-10} mbar using a Phoibos 100 hemispherical analyzer (Specs). As the excitation source a Mg K_α anode was used ($h\nu = 1252.6$ eV, probing depth ~10 nm). Due to charging effects during measurements caused by the low conductivity of the powder samples, the binding energy scale as measured by XPS was shifted by a few electronvolts for the different samples. To account for this, the binding energies were corrected such that adventitious carbon is positioned at 284.8 eV. Integrated peak areas of characteristic core level excitations were used to calculate the embedded amount of SP–O inside the MOF matrices. For this, the peak areas of N, Zn, In, Ga, and Al were evaluated and corrected by their relative sensitivity factors (RSF),[69] as further detailed in the Supporting Information, Table S1.

Solution NMR Experiments

5.5 mg of SP–O@MOF-5 and SP–O@MIL-68(In/Ga) were digested in 1 ml of DMSO-d_6 and 25 µl of DCl were added. Directly after the addition of DCl, the sample was placed in a NMR glass tube. Measurements (ca. 5 min after treatment with DCl) were carried out on a *Bruker Avance DPX 300 NMR* spectrometer with an internal ^{2}D lock. The spectra were recorded at room temperature and processed with *MestReNova 9.0.1-13254*.

UV/vis Spectroscopy

UV/vis spectra of the SP–O@MOF systems were recorded using transparent KBr pellets with a Varian CARY 4000 spectrometer. Transparent pellets were prepared as follows: half a spatula of the substance was carefully ground with six spatulas of dried KBr. The mixture was pressed for 30 min at a pressure of ~530 bar, yielding a thin, transparent, slightly coloured pellet. The KBr pellet was placed into the sample holder, and the sample chamber was evacuated to 10^{-5} mbar. Spectra were recorded before and during irradiation with UV light (λ = 365 nm).

IR Spectroscopy

IR spectra of solid SP–O@MOF-5 were measured with a Nicolet 5700 FT-IR spectrometer using transparent KBr pellets. Transparent pellets were prepared as described for the UV/vis experiments. The KBr pellet was placed into the sample holder, and the sample chamber was evacuated to 10^{-5} mbar. Scans were recorded in the range 360–4000 cm^{-1} with a resolution of 2 cm^{-1}. Ninety scans for each sample were recorded and added. Backgrounds were measured after every sample replacement to ensure the results being as exact as possible. Irradiation times and irradiation wavelengths varied. They are given in the figures of the respective spectra.

DSC/TGA Measurements

DSC/TGA measurements were carried out on a *Mettler Toledo* TGA/DSC 1 Star^e (Al_2O_3 crucible; Ar stream with 30 ml/min; heating rate 5–10 °C/min). Samples of approx. 2–6 mg were weighed out and handled under inert conditions (glovebox) to avoid absorption of humidity.

Acknowledgements

H. A. Schwartz gratefully acknowledges the IPAK grant program of the University of Cologne. The authors thank Johann Pann for fruitful discussions concerning the processing of the NMR results.

Conflict of Interest

The authors declare no conflict of interest.

Keywords: hybrid composite materials · metal-organic frameworks · photochromism · solvatochromism · spirooxazines

[1] S. Castellanos, F. Kapteijn, J. Gascon, *CrystEngComm* **2016**, *18*, 4006–4012.
[2] H. A. Schwartz, U. Ruschewitz, L. Heinke, *Photochem. Photobiol. Sci.* **2018**, *17*, 864–873.
[3] D. Hermann, H. Emerich, R. Lepski, D. Schaniel, U. Ruschewitz, *Inorg. Chem.* **2013**, *52*, 2744–2749.
[4] D. Hermann, *PhD Thesis*, University of Cologne, **2013**.

[5] K. Müller, J. Wadhwa, J. Singh Malhi, L. Schöttner, A. Welle, H. Schwartz, D. Hermann, U. Ruschewitz, L. Heinke, *Chem. Commun.* **2017**, *53*, 8070–8073.
[6] T. Uemura, G. Washino, N. Yanai, S. Kitagawa, *Chem. Lett.* **2013**, *42*, 222–223.
[7] N. Yanai, T. Uemura, M. Inoue, R. Matsuda, T. Fukushima, M. Tsujimoto, S. Isoda, S. Kitagawa, *J. Am. Chem. Soc.* **2012**, *134*, 4501–4504.
[8] D. Hermann, H. A. Schwartz, M. Werker, D. Schaniel, U. Ruschewitz, *Chem. Eur. J.* **2019**, *25*, 3606–3616.
[9] I. M. Walton, J. M. Cox, J. A. Coppin, C. M. Linderman, D. G. (Dan) Patel, J. B. Benedict, H. Ren, G. Zhu, *Chem. Commun.* **2013**, *49*, 8012–8014.
[10] H. A. Schwartz, S. Olthof, D. Schaniel, K. Meerholz, U. Ruschewitz, *Inorg. Chem.* **2017**, *56*, 13100–13110.
[11] F. Zhang, X. Zou, W. Feng, X. Zhao, X. Jing, F. Sun, H. Ren, G. Zhu, *J. Mater. Chem.* **2012**, *22*, 25019–25026.
[12] S. Garg, H. Schwartz, M. Kozlowska, A. B. Kanj, K. Müller, W. Wenzel, U. Ruschewitz, L. Heinke, *Angew. Chem. Int. Ed.* **2019**, *58*, 1193–1197.
[13] Y. Hirshberg, *C. R. Hebd. Seances Acad. Sci.* **1950**, *116*, 903–904.
[14] H. Bouas-Laurent, H. Dürr, *Photochromism* **2003**, *73*, 639–665.
[15] S. R. Batten, N. R. Champness, X.-M. Chen, J. Garcia-Martinez, S. Kitagawa, L. Öhrström, M. O'Keeffe, M. P. Suh, J. Reedijk, *Pure Appl. Chem.* **2013**, *85*, 1715–1724.
[16] C. Zlotea, R. Campesi, F. Cuevas, E. Leroy, P. Dibandjo, C. Volkringer, T. Loiseau, G. Férey, M. Latroche, *J. Am. Chem. Soc.* **2010**, *132*, 2991–2997.
[17] M. P. Suh, H. J. Park, T. K. Prasad, D.-W. Lim, *Chem. Rev.* **2012**, *112*, 782–835.
[18] H. Wu, R. S. Reali, D. A. Smith, M. C. Trachtenberg, J. Li, *Chem. Eur. J.* **2010**, *16*, 13951–13954.
[19] J.-R. Li, J. Sculley, H.-C. Zhou, *Chem. Rev.* **2012**, *112*, 869–932.
[20] L. Alaerts, M. Maes, L. Giebeler, P. A. Jacobs, J. A. Martens, J. F. M. Denayer, C. E. A. Kirschhock, D. E. De Vos, *J. Am. Chem. Soc.* **2008**, *130*, 14170–14178.
[21] M. Maes, F. Vermoortele, L. Alaerts, S. Couck, C. E. A. Kirschhock, J. F. M. Denayer, D. E. De Vos, *J. Am. Chem. Soc.* **2010**, *132*, 15277–15285.
[22] J. Lee, O. K. Farha, J. Roberts, K. A. Scheidt, S. T. Nguyen, J. T. Hupp, *Chem. Soc. Rev.* **2009**, *38*, 1450–1459.
[23] P. Horcajada, T. Chalati, C. Serre, B. Gillet, C. Sebrie, T. Baati, J. F. Eubank, D. Heurtaux, P. Clayette, C. Kreuz, J.-S. Chang, Y. K. Hwang, V. Marsaud, P.-N. Bories, L. Cynober, S. Gil, G. Férey, P. Couvreur, R. Gref, *Nat. Mater.* **2010**, *9*, 172–178.
[24] P. Horcajada, C. Serre, M. Vallet-Regí, M. Sebban, F. Taulelle, G. Férey, *Angew. Chem. Int. Ed.* **2006**, *45*, 5974–5978; *Angew. Chem.* **2006**, *118*, 6120–6124.
[25] V. Stavila, A. A. Talin, M. D. Allendorf, *Chem. Soc. Rev.* **2014**, 5994–6010.
[26] M. D. Allendorf, A. Schwartzberg, V. Stavila, A. A. Talin, *Chem. Eur. J.* **2011**, *17*, 11372–11388.
[27] M. Eddaoudi, J. Kim, N. Rosi, D. Vodak, J. Wachter, M. O'Keeffe, O. M. Yaghi, *Science* **2002**, *295*, 469–472.
[28] K. Ohara, Y. Inokuma, M. Fujita, *Angew. Chem. Int. Ed.* **2010**, *49*, 5507–5509; *Angew. Chem.* **2010**, *122*, 5639–5641.
[29] H. Agarkar, D. Das, *J. Mol. Struct.* **2019**, *1184*, 435–442.
[30] D. Das, H. Agarkar, *ACS Omega* **2018**, *3*, 7630–7638.
[31] O. Chaudé, R. Rumpf, *C. R. Hebd. Seances Acad. Sci.* **1953**, *236*, 697–699.
[32] E. Fischer, Y. Hirshberg, *J. Chem. Soc.* **1952**, 4522–4524.
[33] V. Lokshin, A. Samat, A. V. Metelitsa, *Russ. Chem. Rev.* **2002**, *71*, 893–916.
[34] D. E. Williams, C. R. Martin, E. A. Dolgopolova, A. Swifton, D. C. Godfrey, O. A. Ejegbavwo, P. J. Pellechia, M. D. Smith, N. B. Shustova, *J. Am. Chem. Soc.* **2018**, *140*, 7611–7622.
[35] E. A. Dolgopolova, V. A. Galitskiy, C. R. Martin, H. N. Gregory, B. J. Yarbrough, A. M. Rice, A. A. Berseneva, O. A. Ejegbavwo, K. S. Stephenson, P. Kittikhunnatham, S. G. Karakalos, M. D. Smith, A. B. Greytak, S. Garashchuk, N. B. Shustova, *J. Am. Chem. Soc.* **2019**, *141*, 5350–5358.
[36] D. E. Williams, J. A. Rietman, J. M. Maier, R. Tan, A. B. Greytak, M. D. Smith, J. A. Krause, N. B. Shustova, *J. Am. Chem. Soc.* **2014**, *136*, 11886–11889.
[37] C. C. Epley, K. L. Roth, S. Lin, S. R. Ahrenholtz, T. Z. Grove, A. J. Morris, *Dalton Trans.* **2017**, *46*, 4917–4922.
[38] J. Zhang, L. Wang, N. Li, J. Liu, W. Zhang, Z. Zhang, N. Zhou, X. Zhu, *CrystEngComm* **2014**, *16*, 6547–6551.
[39] A. Schaate, S. Dühnen, G. Platz, S. Lilienthal, A. M. Schneider, P. Behrens, *Eur. J. Inorg. Chem.* **2012**, *2012*, 790–796.
[40] Y. Zheng, H. Sato, P. Wu, H. J. Jeon, R. Matsuda, S. Kitagawa, *Nat. Commun.* **2017**, *8*, 100 (1–6).
[41] J. Park, D. Yuan, K. T. Pham, J.-R. Li, A. Yakovenko, H.-C. Zhou, *J. Am. Chem. Soc.* **2012**, *134*, 99–102.
[42] X. Yu, Z. Wang, M. Buchholz, N. Füllgrabe, S. Grosjean, F. Bebensee, S. Bräse, C. Wöll, L. Heinke, *Phys. Chem. Chem. Phys.* **2015**, *17*, 22721–22725.
[43] A. Modrow, D. Zargarani, R. Herges, N. Stock, *Dalton Trans.* **2011**, *40*, 4217–4222.
[44] A. Modrow, D. Zargarani, R. Herges, N. Stock, *Dalton Trans.* **2012**, *41*, 8690–8696.
[45] L. Heinke, M. Cakici, M. Dommaschk, S. Grosjean, R. Herges, S. Bräse, C. Wöll, *ACS Nano* **2014**, *8*, 1463–1467.
[46] L. Heinke, *J. Phys. D. Appl. Phys.* **2017**, *50*, 193004 (1–18).
[47] K. Müller, J. Helfferich, F. Zhao, R. Verma, A. B. Kanj, V. Meded, D. Bléger, W. Wenzel, L. Heinke, *Adv. Mater.* **2018**, *30*, 1706551 (1–7).
[48] Z. Wang, L. Heinke, J. Jelic, M. Cakici, M. Dommaschk, R. J. Maurer, H. Oberhofer, S. Grosjean, R. Herges, S. Bräse, K. Reuter, C. Wöll, *Phys. Chem. Chem. Phys.* **2015**, *17*, 14582–14587.
[49] K. Healey, W. Liang, P. D. Southon, T. L. Church, D. M. D'Alessandro, *J. Mater. Chem. A* **2016**, *4*, 10816–10819.
[50] Z. Wang, K. Müller, M. Valášek, S. Grosjean, S. Bräse, C. Wöll, M. Mayor, L. Heinke, *J. Phys. Chem. C* **2018**, *122*, 19044–19050.
[51] H. Li, M. Eddaoudi, M. O'Keeffe, O. M. Yaghi, *Nature* **1999**, *402*, 276–279.
[52] C. Volkringer, M. Meddouri, T. Loiseau, N. Guillou, J. Marrot, G. Férey, M. Haouas, F. Taulelle, N. Audebrand, M. Latroche, *Inorg. Chem.* **2008**, *47*, 11892–11901.
[53] T. Loiseau, C. Serre, C. Huguenard, G. Fink, F. Taulelle, M. Henry, T. Bataille, G. Férey, *Chem. Eur. J.* **2004**, *10*, 1373–1382.
[54] V. Petříček, M. Dušek, L. Palatinus, *Jana2006: The Crystallographic Computing System*, Institute Of Physics, Praha: The Czech Republic, **2006**.
[55] J. Yang, A. Grzech, F. M. Mulder, T. J. Dingemans, *Chem. Commun.* **2011**, *47*, 5244–5246.
[56] L. Kortekaas, W. R. Browne, *Chem. Soc. Rev.* **2019**, *48*, 3406–3424.
[57] L. Kortekaas, J. Chen, D. Jacquemin, W. R. Browne, *J. Phys. Chem. B* **2018**, *122*, 6423–6430.
[58] R. Klajn, *Chem. Soc. Rev.* **2014**, *43*, 148–184.
[59] A. A. Rezvanova, L. A. Frolova, P. A. Troshin, *Mendeleev Commun.* **2016**, *26*, 26–28.
[60] T. Ubukata, S. Fujii, K. Arimatsu, Y. Yokoyama, *J. Mater. Chem.* **2012**, *22*, 14410–14417.
[61] J. Harada, Y. Kawazoe, K. Ogawa, *Chem. Commun.* **2010**, *46*, 2593–2595.
[62] P. L. Gentili, M. Nocchetti, C. Miliani, G. Favaro, *New J. Chem.* **2004**, *28*, 379–386.
[63] G. Arnold, G. Paal, *Tetrahedron* **1971**, *27*, 1699–1713.
[64] L. L. Gladkov, Y. D. Khamchukov, I. Y. Sychev, A. V. Lyubimov, *J. Appl. Spectrosc.* **2012**, *79*, 31–37.
[65] M. Hesse, H. Meyer, B. Zeeh, *Spektroskopische Methoden in Der Organischen Chemie*, Georg Thieme Verlag, Stuttgart, **2002**.
[66] F. Maurel, J. Aubard, M. Rajzmann, R. Guglielmetti, A. Samat, *J. Chem. Soc. Perkin Trans. 2* **2002**, *0*, 1307–1315.
[67] T. Horii, Y. Abe, R. Nakao, *J. Photochem. Photobiol. A* **2001**, *144*, 119–129.
[68] D. J. Tranchemontagne, J. R. Hunt, O. M. Yaghi, *Tetrahedron* **2008**, *64*, 8553–8557.
[69] J. H. Scofield, *J. Electron Spectrosc. Relat. Phenom.* **1976**, *8*, 129–137.

Manuscript received: July 18, 2019
Revised manuscript received: November 11, 2019
Accepted manuscript online: December 10, 2019
Version of record online: January 9, 2020